nature physics

ARTICLES

PUBLISHED ONLINE: 24 APRIL 2011 | DOI: 10.1038/NPHYS1988

Microscopic polarization in bilayer graphene

Gregory M. Rutter[1†], Suyong Jung[1,2†], Nikolai N. Klimov[1,2,3], David B. Newell[3], Nikolai B. Zhitenev[1*] and Joseph A. Stroscio[1*]

Bilayer graphene contains, compared to single-layer graphene, additional states related to the symmetry of the layers. These states can lead to the opening of a bandgap, which is highly desirable for device applications. The gap can be either tunable through an external electric field or spontaneously formed through an interaction-induced symmetry breaking. Here, we report scanning tunnelling microscopy measurements that reveal that the microscopic nature of the bilayer gap is very different from what has been observed in previous macroscopic measurements, and from what is expected from current theoretical models. The potential difference between the layers, which is proportional to charge imbalance and determines the gap value, shows a strong dependence on the disorder potential and varies spatially in both magnitude and sign on a microscopic level. Additional interaction-induced effects are observed on applying a magnetic field, as a subgap opens once the zero-orbital Landau level is placed at the Fermi energy.

Bilayer graphene consists of two graphene sheets overlaid in the Bernal stacking orientation, where $\mathbf{A}_2$ atoms of the top layer lie on top of the $\mathbf{B}_1$ atoms of the bottom layer (see Fig. 1a), connected by the interlayer coupling γ_1, thus breaking the $\mathbf{A}/\mathbf{B}$ sublattice symmetry in the individual graphene layers. This results in massive chiral fermions, where the electronic energy dispersion is hyperbolic in momentum, in contrast to the linear dispersion that leads to massless carriers in single layer graphene[1,2]. In bilayer graphene the energy bands still meet at the charge neutrality point (E_D) in the absence of an electric field between the layers (neglecting interaction effects) (Fig. 1b). In an applied electric field a potential asymmetry is developed between the layers, resulting in the opening of an energy bandgap between the low-lying bands and making bilayer graphene of great interest for electronic applications (Fig. 1b; refs 2–10). Bilayer graphene also differs from single layer graphene in its magnetic quantization in the quantum Hall regime. At E_D, the four-fold degenerate Landau level (LL) in single layer graphene becomes eight-fold degenerate in bilayer graphene because of the additional layer degeneracy[3,11,12]. When the gap is opened this manifold splits into two four-fold degenerate quartets polarized on each layer at low energies. Lifting of these degeneracies has been observed in recent measurements[13–16]. Theoretical studies[17,18] suggest the existence of interaction-driven bandgaps, which are even possible in zero applied field with corresponding quantum Hall ferromagnetic states[18,19].

The energy bandgap in bilayer graphene has been observed using optical measurements, such as angle resolved photoemission spectroscopy[20] and infrared spectroscopy[4–6,21], which have demonstrated that the gap is externally tunable and can reach values up to ≈250 meV. However, the bandgaps determined from conventional electronic transport measurements vary greatly and can be much smaller than those theoretically expected or extracted from the optical measurements[7,8,13,22–25]. Recently, it has been suggested that disorder-induced localized states inside the devices or along the edges can introduce extra conducting channels inside the gap, consequently reducing the effective gap seen in transport measurements[23–25]. Furthermore, many-body interactions in bilayer graphene are expected to open a gap even in zero applied field[11,18]. Accordingly, the interplay between the interactions, external and disorder-induced local electric fields, and localized states in the gap is becoming the central issue in the physics of the bilayer graphene system.

In this article, we present scanning tunnelling microscopy (STM) and scanning tunnelling spectroscopy (STS) measurements of a gated bilayer graphene device in magnetic fields ranging from zero to the quantum Hall regime. We investigate the local density of states and the formation of an energy bandgap affected by disorder while tuning the total charge density, as the Fermi energy (E_F) is varied with an electrostatic back gate with respect to E_D. Surprisingly, the local potential difference determined between the layers, which defines the gap, does not follow the previously reported electrostatic models[2,7], which predict that an external electric field is the main parameter controlling the asymmetries of the bilayer potential. We observe the spatial variation of the potential difference to be highly correlated with the disorder potential.

The experimental set-up is shown schematically in Fig. 1c. The topographic height fluctuations on the bilayer (Fig. 2b) are dominated by the underlying SiO_2 surface roughness, as they are in the single layer[26–28]. We have obtained the spatial profile of the bilayer disorder potential (Fig. 2c) over the 100 nm × 100 nm topographic region shown in Fig. 2b. The red and blue coloured areas are the regions of low and high disorder potential, which correspond to electron and hole puddles at near-zero carrier density, respectively. For brevity, we will refer to the disorder extrema as electron and hole puddles at arbitrary carrier densities for the rest of this manuscript. We note that the size of the puddles in the bilayer is significantly smaller than that in the single layer with the corresponding impurity density[28]; ≈10 nm in the bilayer compared with ≈30 nm in the single layer.

We first discuss the measurements of the bilayer gap in zero magnetic field, followed by the measurements at high magnetic fields in both electron and hole puddles. Figure 3a shows a sequence of $\mathrm{d}I/\mathrm{d}V$ spectra at gate voltages ranging from 0 to 60 V, obtained

[1]Center for Nanoscale Science and Technology, NIST, Gaithersburg, Maryland 20899, USA, [2]Maryland NanoCenter, University of Maryland, College Park, Maryland 20742, USA, [3]Physical Measurement Laboratory, NIST, Gaithersburg, Maryland 20899, USA. †These authors contributed equally to this work. *e-mail: nikolai.zhitenev@nist.gov; joseph.stroscio@nist.gov.

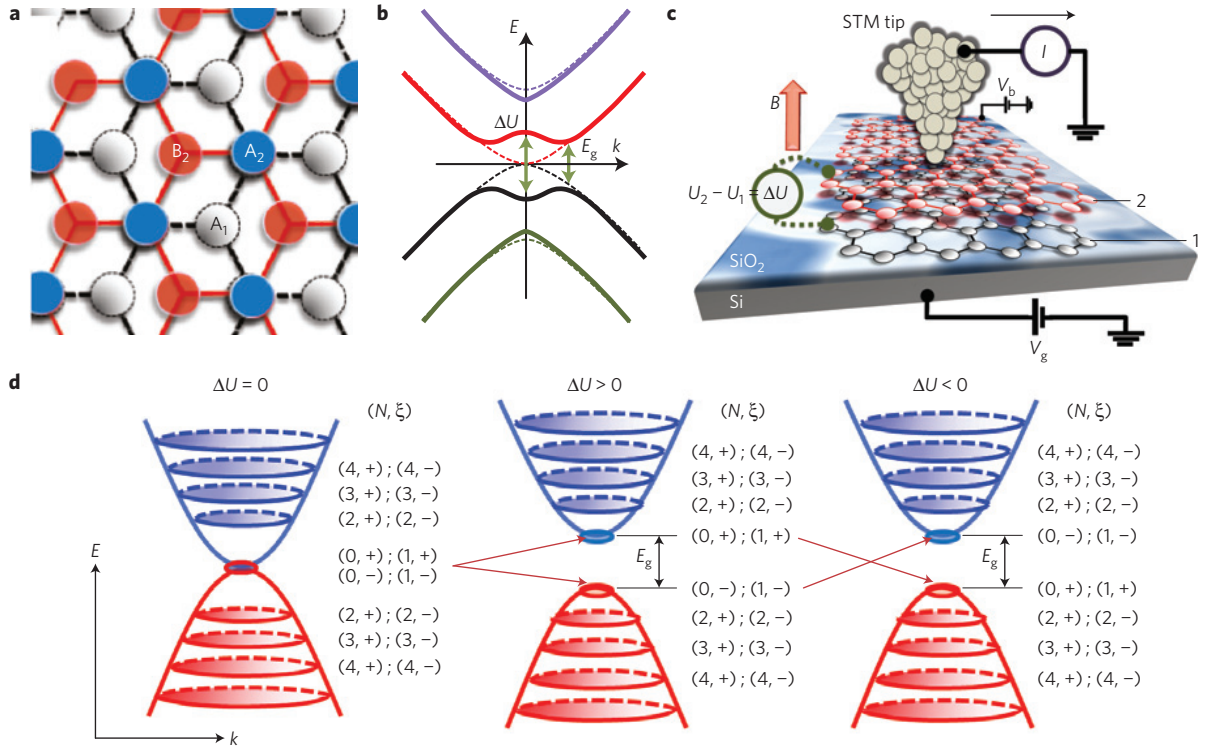

Figure 1 | Schematics of the bilayer graphene measurements and energy band diagrams in the quantum Hall regime. a, Schematic of Bernal-stacked bilayer graphene consisting of a top layer ($\mathbf{A}_2/\mathbf{B}_2$) and bottom layer ($\mathbf{A}_1/\mathbf{B}_1$), with atom $\mathbf{A}_2$ directly over $\mathbf{B}_1$. **b**, Energy band diagram of bilayer graphene with (solid lines) and without (dashed lines) a bandgap. The electronic levels form Mexican-hat like energy bands with a potential energy asymmetry ΔU and a bandgap of E_g. **c**, Schematic of a gated bilayer graphene device for STM/STS measurement with circuitry showing the application of the gate voltage V_g and sample bias V_b. The bilayer graphene is placed on a 300 nm SiO_2 substrate separating it from a back gate electrode (Si) (see Methods). The disorder potential induced by the substrate is illustrated in colour, overlaid on the SiO_2 surface. ΔU is the difference between the onsite energies for the top (2) and the bottom (1) layers. Magnetic field B is perpendicular to the sample plane. **d**, The formation of bilayer graphene Landau levels in the quantum Hall regime with and without a bandgap. Landau levels are indexed by the orbital and valley index, (N, ξ), and each is two-fold degenerate in spin. The eight-fold degenerate $N = 0, 1$ levels become layer-polarized quartets when the graphene layers are subjected to a potential energy asymmetry ΔU. $LL_{(0,+);(1,+)}$ projected on the top layer ($\xi = +1$) depends on the sign of ΔU.

in the electron puddle denoted by P1 in Fig. 2c. In Fig. 3b, we use a colour-coded gate map to plot the STS spectra obtained with finer steps in gate potential, as previously applied to single layer graphene[28]. At $V_g = 0$ V, we observe two main minima in the tunnelling spectra (marked with red and orange tick marks in Fig. 3a), one at E_F and one at 80 mV. The gap at E_F is characteristic of tunnelling into low-dimensional systems[29], and we associate the minimum centred at 80 mV with the bandgap of bilayer graphene. Because of the multiple peaks seen in the sequence of spectra in Fig. 3a, which we relate to scattering resonances in the disorder potential[28], the reliable assignment of the bilayer bandgap is possible only after careful study of the zero field gate map in Fig. 3b and the magnetic field dependent measurements, such as the ones displayed in Fig. 3e–g. The minima associated with the bilayer gaps are observed to increase in energy width as a function of magnetic field (Fig. 3e–g), with the development of Landau levels, as expected (see discussion below). Once the gap is identified, it can be tracked as a function of gate voltage, as shown by the orange tick marks in Fig. 3a and green circles in Fig. 3b. Furthermore, we determine the edges of the gap as the closest peaks on either side of the gap minima (indicated by the red and blue dots in Fig. 3b). The charge neutrality point (green circles in Fig. 3b) can be extracted from the centre of the gap, which leads to an estimate of the effective mass and the Fermi velocity of bilayer graphene (see Methods).

We now discuss the bilayer spectrum in the quantum Hall regime at high magnetic fields. In the presence of a perpendicular magnetic field B, the massive chiral fermions in gapless bilayer graphene are quantized with energies $E_N = \pm\hbar\omega_c\sqrt{N(N-1)}, N = 0, 1, 2, \ldots$, where $\hbar$ is Planck's constant, $\omega_c = eB/m^*$ is the cyclotron frequency, and e is the electron charge[12,30]. For each orbital quantum number, N, the Landau levels (LL_N) are four-fold degenerate owing to the degeneracy of valleys $\mathbf{K}$ and $\tilde{\mathbf{K}}$, with respective quantum numbers $\xi = +1$ and $\xi = -1$, and spin degeneracy $s = \uparrow, \downarrow$. In the absence of both an applied electric field and interactions, the $N = 0$ and $N = 1$ LLs are further degenerate, with an eight-fold degeneracy occurring at $E_{N=0,1} = 0$ meV. In the presence of an applied electric field this degeneracy is partially lifted and a bandgap is opened in the low-energy bands. Accordingly, the Landau level energies are modified to[3,11,12]

$$E_N = \pm\hbar\omega_c\sqrt{N(N-1) + (\Delta U/2\hbar\omega_c)^2} - \frac{1}{4}\xi z\Delta U, \quad N = 2, 3, 4\ldots \tag{1}$$

$$E_{N=0} = \xi\Delta U/2, \quad E_{N=1} = \xi(\Delta U/2)(1-z)$$

with the potential energy difference (or asymmetry) $\Delta U = U_2 - U_1$, where U_2 and U_1 are the onsite energies of the top and bottom graphene layers, respectively (Fig. 1c), and z is a term relating to the $\mathbf{B}_2/\mathbf{A}_1$ dimer sites, given by $z = 2\hbar\omega_c/\gamma_1 \ll 1$. For $\Delta U < \gamma_1$, the absolute value of the potential energy asymmetry is approximately equal to the bandgap, $|\Delta U| \approx E_g$ (see Fig. 1b). As z is small for typical magnetic fields ($B \leq 8$ T), the $N = 0$ and $N = 1$ LLs are almost degenerate. We label these states as $LL_{(N,\xi=\pm)}$, with orbital

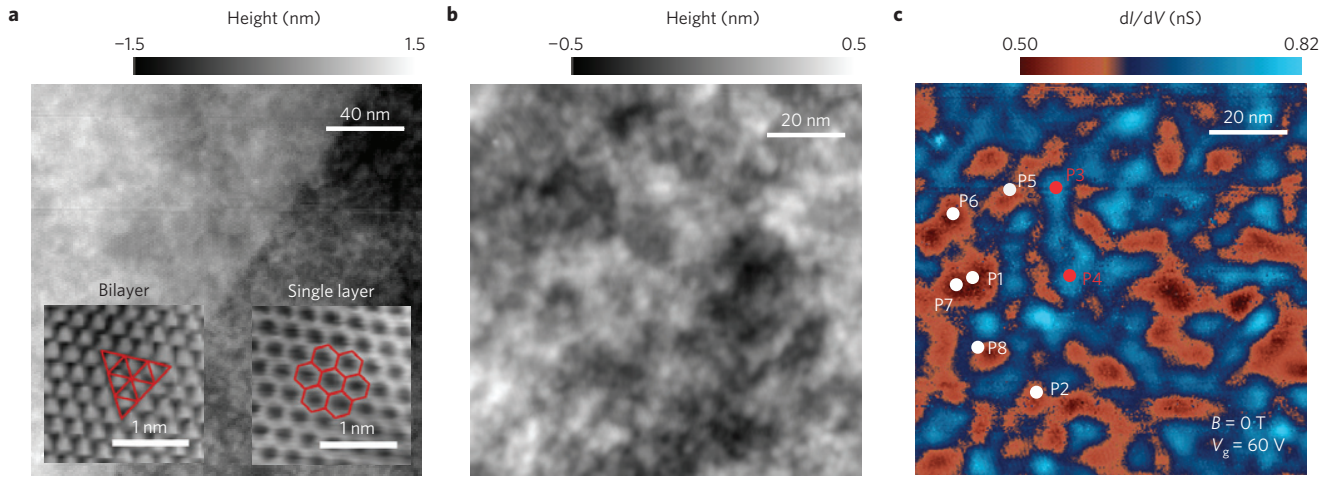

Figure 2 | STM topography images and disorder potential in bilayer graphene. a, STM topographic image, 200 nm × 200 nm, of a region containing the boundary between single and bilayer graphene. Tunnelling parameters: sample bias −300 mV, tunnelling current 100 pA. Lower right inset: atomic resolution image of the honeycomb lattice structure of single layer graphene. Lower left inset: atomic resolution image of the bilayer showing the three-fold symmetry of Bernal-stacked bilayer graphene. **b**, STM topographic image, 100 nm × 100 nm, of bilayer graphene with a peak-to-peak height corrugation of 1 nm. Tunnelling parameters: sample bias −200 mV, tunnelling current 300 pA. **c**, Fixed-bias closed-loop dI/dV map ($V_b = -200$ mV, $V_g = 60$ V), over the same area as in **b**, showing the spatial distribution of the disorder potential in bilayer graphene. Different measurement points, six for electron puddles (white circles) and two for hole puddles (red circles) are indicated.

and valley indices N and $\xi = \pm$, but without the spin index label. Landau levels that are degenerate at different orbital indices (N and N') are separated by a semicolon in the notation as $\mathrm{LL}_{(N,\pm);(N',\pm)}$.

Significantly, the spinor states related to the $N = 0$ and $N = 1$ states in the $\tilde{\mathbf{K}}(\xi = -1)$ valley ($\mathrm{LL}_{(0,-);(1,-)}$) are localized predominantly on the $\mathbf{A}_1$ sites of the bottom layer, whereas those of the $N = 0$ and $N = 1$ states in the $\mathbf{K}$ ($\xi = +1$) valley ($\mathrm{LL}_{(0,+);(1,+)}$) are localized on the $\mathbf{B}_2$ sites of the top layer[11,12]. This layer polarization is of particular importance in the STS measurements, as tunnelling to the top surface layer dominates the dI/dV spectra. Analysis of the state, $\mathrm{LL}_{(0,+);(1,+)}$, which resides predominantly in the top layer and belongs either to the valence band ($\Delta U < 0$) or to the conduction band ($\Delta U > 0$) (Fig. 1d) enables us to determine both the sign and the value of ΔU.

A rich set of spectral features is observed in the STS spectra of bilayer graphene in the quantum Hall regime. Figure 3c shows the gate map at the location of electron puddle P1 (Fig. 2c) at 8 T. Resonance peaks from impurity scattering become suppressed as graphene charge carriers are condensed into LLs. The bright lines in Fig. 3c represent well-defined LLs, observed up to $\mathrm{LL}_{N=6}$ for both electron and hole doping. A staircase-like pattern is observed in the LL transitions as a function of gate voltage, which results from the LL pinning at E_F (ref. 28), and is characteristic of a two-dimensional electron gas in high magnetic fields[31]. A large gap in the dI/dV spectrum is observed in the gate map (Fig. 3c) as a function of gate voltage, with two prominent LLs on either side of the gap. For comparison, the bandgap edges observed at zero magnetic field are overlaid on the map (red and blue dots) in Fig. 3c. To identify the orbital index N of each LL, we examine the magnetic field dependence of the dI/dV spectra and LL peak positions shown in Fig. 3e. In the electron puddles, a prominent LL is observed to grow out of the lower energy side of the gap, with minimal dispersion in magnetic field. This LL belongs to the valence band, and we identify it as $\mathrm{LL}_{(0,+);(1,+)}$, which resides in the top graphene layer at high magnetic field. The corresponding level $\mathrm{LL}_{(0,-);(1,-)}$, residing on the bottom layer, is not observed, as the tunnelling probability from the probe tip to this layer is exponentially decreased. The same level assignment is valid for the whole gate voltage range. With the $\mathrm{LL}_{(0,+);(1,+)}$ quartet assigned, the other LLs at higher orbital indices can be indexed accordingly, as marked in Fig. 3e.

The bilayer bandgap varies considerably on a microscopic level. Figure 3d shows the spectral gate map measured at the position of a hole puddle ('P4' in Fig. 2c), which can be contrasted with the measurements in Fig. 3c of an electron puddle ('P1' in Fig. 2c). The spectra in the electron and hole puddles are reproducibly distinct, as can be seen from the comparison of another pair of electron and hole puddles in Fig. 4b,c. Similar to single layer graphene[28], when the LLs are pinned at E_F, the gate maps show LL transitions that display convex curvature for the hole puddles (Figs 3d and 4b) and concave curvature for the electron puddles (Figs 3c and 4c). Comparing the spectral peaks for the electron puddles with those for hole puddles we observe a striking difference in the layer-polarized LLs. As shown in Fig. 3f, the strong non-dispersive $\mathrm{LL}_{(0,+);(1,+)}$ grows out of the higher energy side of the bilayer gap at the conduction band edge (blue dots in Fig. 3d), as opposed to the lower energy side of the valence band as for electron puddles (Fig. 3e). This indicates a reversal in the sign of the electric field between the graphene layers and results in a sign change of the energy asymmetry, ΔU (see Fig. 1c).

From the LL spectral peak positions, we can quantitatively determine the values of the bilayer energy gap in different puddles from equation (1), using the energy asymmetry ΔU and the Fermi-velocity v_F as fitting parameters. The dark brown tick marks in Fig. 3e (Fig. 3f) indicate the fitted LL positions from equation (1) using an energy asymmetry $\Delta U = -34.8$ meV ($\Delta U = 31.9$ meV), and Fermi velocity $v_F = 1.00 \times 10^6$ m s^{-1} ($v_F = 1.01 \times 10^6$ m s^{-1}) for electron (hole) puddle P1 (P4). In Fig. 3g, the fan diagram (solid lines) generated with the fit parameters for puddle P1 shows how individual LLs are expected to evolve as a function of magnetic field, along with experimental LL energies (red squares) for the field range from 2 to 8 T and the bandgap edges determined at 0 T. Fairly good agreement is observed over the entire field range using the gap and velocity values obtained by fitting the 8 T spectra alone. Better agreement between the model and measured LL energies can be obtained by fitting the energy asymmetry and velocity for each magnetic field.

The extracted ΔU values at 6 and 8 T as a function of gate voltage are shown in Fig. 4a, together with ΔU measured in zero field, for electron puddle P1 and hole puddle P4. We note that ΔU qualitatively follows the separation between $\mathrm{LL}_{(0,+);(1,+)}$ and

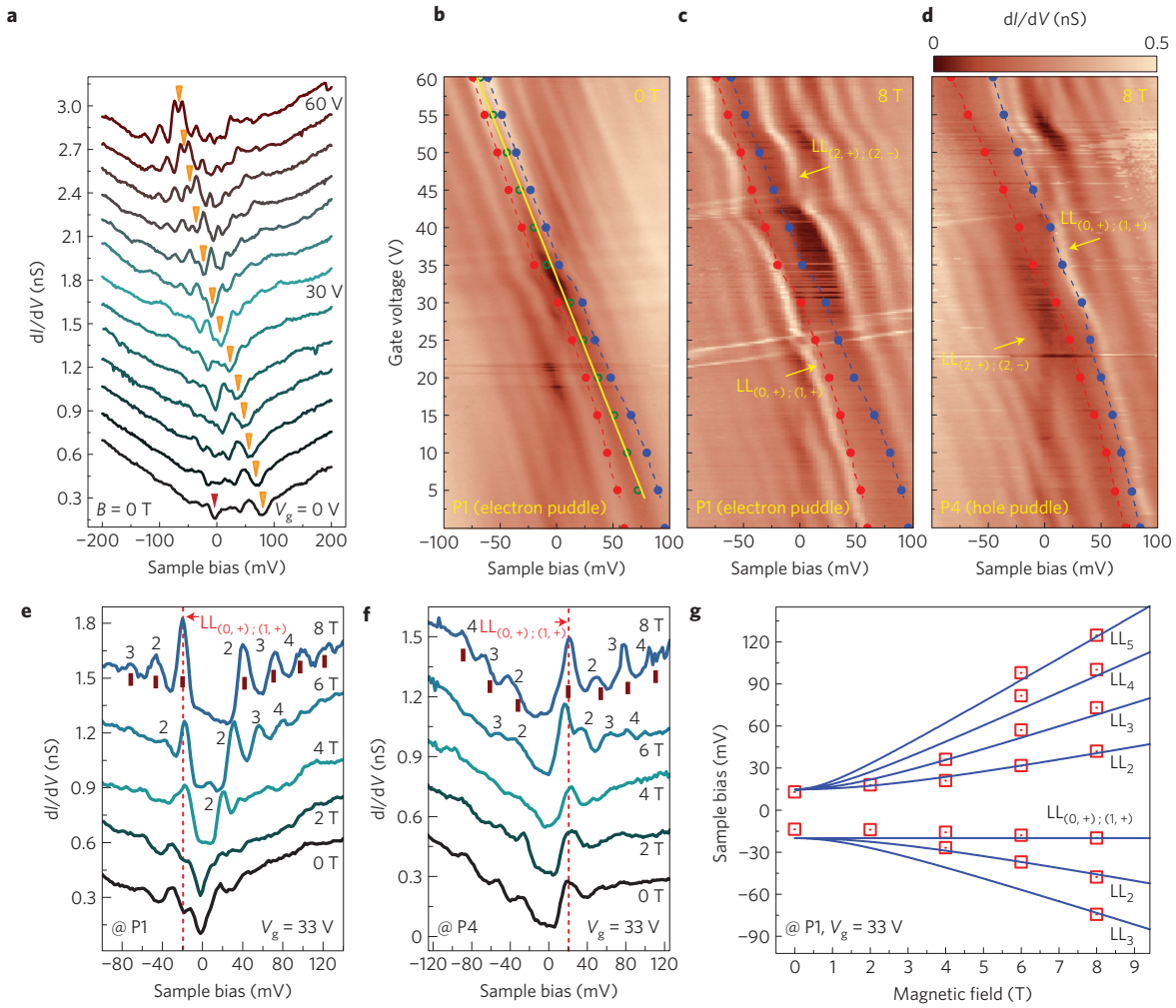

Figure 3 | Magnetic quantization in bilayer graphene as a function of electric and magnetic fields. a, dI/dV spectra in zero magnetic field as a function of back gate voltage in steps of $\Delta V_g = 5$ V in electron puddle P1. The curves are offset for clarity. The red tick mark at $V_g = 0$ V indicates the conductance minimum at E_F and the orange tick marks indicate the minima of the bilayer bandgap as a function of gate voltage. **b**, two-dimensional 'gate map' from dI/dV spectra with finer gate voltage increments ($\Delta V_g = 0.2$ V). The green circles show the position of the charge neutrality point, E_D, in the centre of the gap and the yellow line is a linear fit of E_D versus gate voltage, which yields an effective mass $m^* = (0.033 \pm 0.002)m_e$ (all uncertainties reported represent one standard deviation in the measured quantity; see Methods). The red and blue connected dots denote the edges of the bandgap. **c**, dI/dV gate map measured at 8 T at the same location as **a** and **b** (P1). The red and blue connected dots are the same as in **b**. **d**, dI/dV gate map measured at 8 T at the position of hole puddle P4. The red and blue connected dots denote the gap edges of the hole puddle determined from zero field measurements. **e**,**f**, Individual dI/dV spectra for electron puddle P1 and hole puddle P4, respectively, as a function of applied magnetic field from 0 to 8 T at a fixed gate voltage of $V_g = 33$ V. The curves are offset for clarity. Dark brown tick marks show LL positions for each puddle calculated using equation (1). STS parameters (**a**–**f**): sample bias −200 mV, tunnelling current 200 pA and root-mean-square modulation voltage 4 mV. **g**, Landau level peak positions (red squares) as a function of magnetic field for electron puddle P1 at $V_g = 33$ V (error bars smaller than symbol size). The experimental points at 0 and 2 T are extracted from the bandgap edges.

$LL_{(2,+);(2,-)}$, which can be seen directly from the gate maps in Fig. 3c,d (see also Supplementary Information). Interestingly, the ΔU dependence on density shows an almost mirror symmetry about zero energy for electron ($\Delta U < 0$) and hole ($\Delta U > 0$) puddles. The magnitude of ΔU is comparable at opposite ends of the doping range. The energy difference measured in the electron puddle at $V_g = 0$ V is ≈ -35 meV. For the hole puddle, the energy difference is $\approx +35$ meV at $V_g = 60$ V. Furthermore, it is interesting to note that the energy difference at low gate voltage ($0\,\text{V} < V_g < 20\,\text{V}$) follows the energy difference measured in zero magnetic field for the electron puddle. For the hole puddle, however, the energy difference in higher magnetic fields matches those in zero field at high gate voltage ($40\,\text{V} < V_g < 60\,\text{V}$). In addition, there is a series of dips (peaks) in the electron (hole) energy asymmetries at higher (lower) gate voltage, each corresponding to the transitions of the various LLs through E_F. The peak at $V_g = 27$ V in hole puddle data corresponds to the filling of $LL_{(2,+);(2,-)}$. In comparison, in the electron puddle data the dips at $V_g = 40$ V and $V_g = 50$ V correspond respectively to the filling of $LL_{(2,+);(2,-)}$ and $LL_{(3,+);(3,-)}$ at E_F. Coincident with the variation in the gap size is a variation of a few per cent in the value of the Fermi velocity (see Supplementary Information).

We compare the observed density dependence of ΔU with the zero-magnetic field calculations (blue line in Fig. 4a) using a tight-binding model with a self-consistent Hartree approximation[2]. The model predicts a vanishing ΔU and sign reversal at E_D. The models[11,12] describing the bilayer band structure in a high magnetic field are not self-consistent and implicitly assume an energy asymmetry dependence on the gate electric field, illustrated by the dashed blue line in Fig. 4a. Here, the energy gap opens

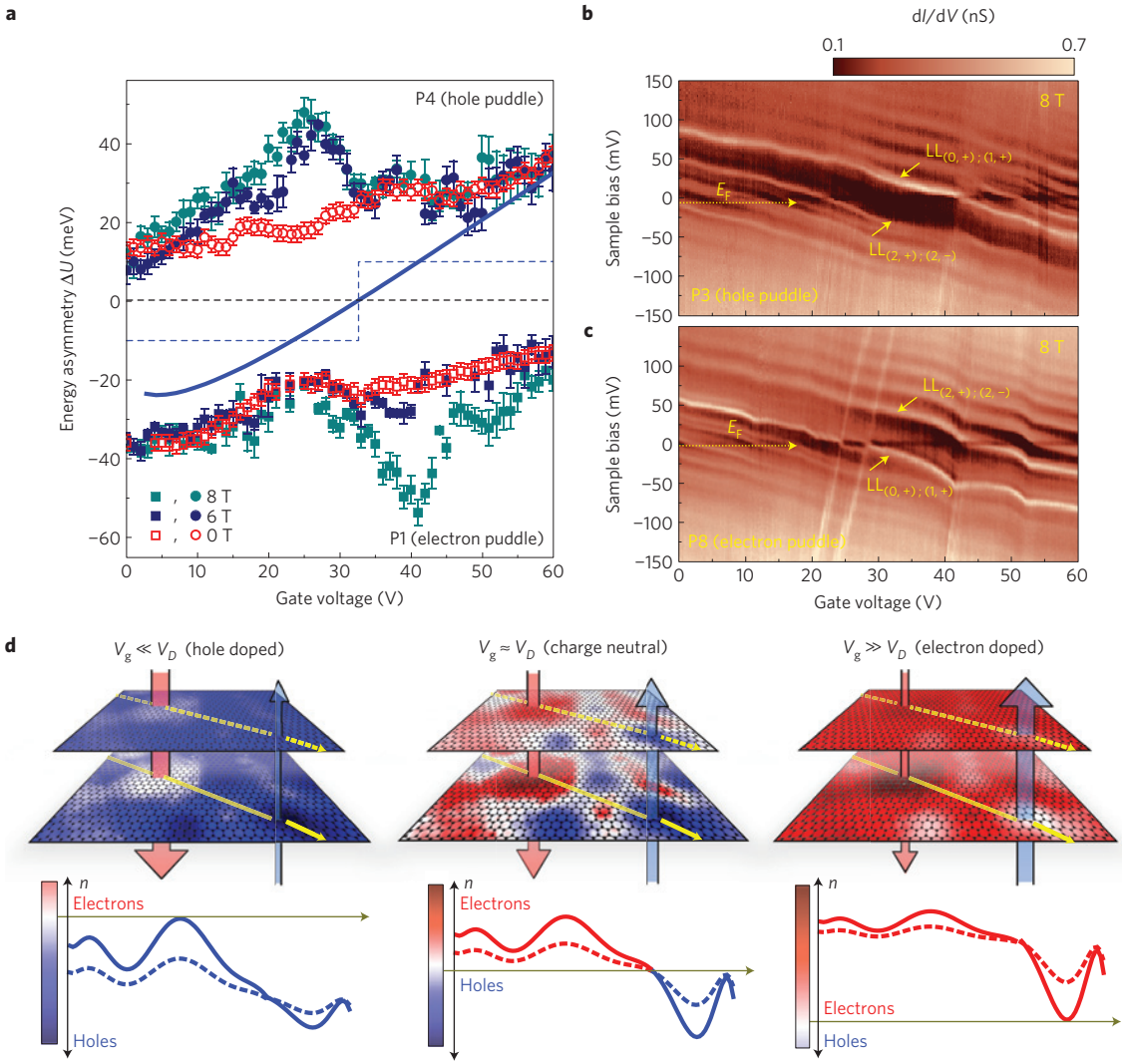

Figure 4 | Bilayer graphene potential energy asymmetries at varying gate voltage for electron and hole puddles. a, Energy asymmetries determined from fitting the LLs using equation (1) as a function of gate voltage and magnetic field obtained at the spatial location of electron puddle P1 and hole puddle P4. Error bars are one standard deviation. The solid blue line indicates the asymmetry in potential calculated using Eq. 5 in ref. 9 with $\Delta_0 = -76$ meV, $v_F = 1.00 \times 10^6$ m s^{-1}, and $\varepsilon_r = 1$. The dashed blue line is the asymmetry dependence implied in the LL scheme illustrated in Fig. 1d. **b**,**c**, Comparison of dI/dV gate maps at 8 T measured in hole puddle P3 (**b**) and electron puddle P8 (**c**). STS parameters: sample bias −200 mV, tunnelling current 200 pA and root-mean-square modulation voltage 4 mV. **d**, Schematics of the spatial inhomogeneity of the layer densities in bilayer graphene at different gate potentials according to the observations made in **a**. The plots on the bottom illustrate the density variation in both top (dashed line) and bottom (solid line) layers along the direction marked by the yellow arrows above. The amplitude of density fluctuations is smaller in the top layer because of the screening from the bottom layer. The direction of the electric field between the layers and the sign of the energy asymmetry remains the same over the whole density range explored.

and the layer polarization develops when E_D crosses E_F, whereas LLs with higher orbital indices, $N \geq 2$, are not layer polarized and therefore do not contribute to changes in relative charge imbalance or the asymmetry size. In contrast, our observations show strong peaks and dips in the energy difference when higher orbital LLs are filled or emptied. It is clear that the experimental observations presented in this manuscript are very different from what either model predicts.

A gap (or subgap) of another type is seen as a splitting of $LL_{(0,+);(1,+)}$ when it crosses E_F. The splitting has been observed in all six examined electron puddle locations marked in Fig. 2c. The splitting of $LL_{(0,+);(1,+)}$ at E_F is also seen as resonances that appear as nearly vertical lines in the gate maps (see Figs 4c and 5a). The presence of vertical resonances in the gate maps has been discussed in a recent study on single layer graphene[28], where we showed that the physical phenomena at E_F can also contribute to the dI/dV spectra at higher tunnelling energies. The resonances occur when the split $LL_{(0,+);(1,+)}$ levels are pulled through the Fermi level at high tip–sample potentials, giving a step increase in tunnelling current and a resonance peak in the dI/dV measurements[32].

The splitting of $LL_{(0,+);(1,+)}$ at E_F is a sign of correlated electron behaviour[33]. The inset in Fig. 5b shows an individual dI/dV spectrum for electron puddle P2 in the middle of the subgap, at $V_g = 28.6$ V. The four-fold degeneracy of $LL_{(0,+);(1,+)}$ is partially lifted and it splits into two peaks separated by 15.4 meV at 8 T. The gap is almost constant and collapses suddenly when $LL_{(0,+);(1,+)}$ is moved away from E_F. The peak separation scales linearly with magnetic field, with a slight variation between different puddles, as shown in Fig. 5b. Fitting the splitting energies to a Zeeman-like dependence, $E = g\mu_B B$, yields an extremely large energy scale for the splitting, $\approx$1.97 meV T^{-1}, with effective $g \approx 34$ for puddle P2, and $\approx$1.70 meV T^{-1}, with $g \approx 29$ for puddle P1. Interestingly, such

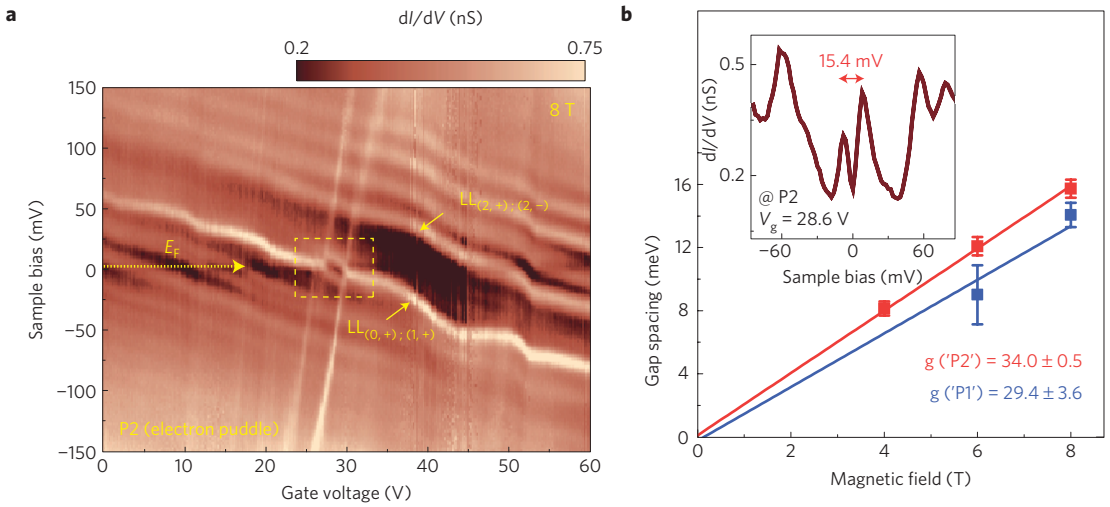

Figure 5 | Symmetry breaking in the $LL_{(0,+);(1,+)}$ quartet. a, dI/dV gate map at 8 T in electron puddle P2. $LL_{(0,+);(1,+)}$ is observed to split into two peaks, opening a subgap when intersecting E_F inside the dashed black rectangle. STS parameters: sample bias −200 mV, tunnelling current 200 pA and root-mean-square modulation voltage 4 mV. **b**, The subgap energy versus magnetic field for electron puddles P1 and P2. A linear fit of the gap versus magnetic field yields slopes of (1.70 ± 0.21) meV T^{-1} and (1.97 ± 0.03) meV T^{-1} for positions P1 and P2, respectively. (Inset) dI/dV spectra in the middle of the subgap of electron puddle P2, at $V_g = 28.6$ V, as marked in the gate map (**a**), showing the subgap size of 15.4 meV at 8 T.

subgaps are not resolved in the hole puddles (see Fig. 4b), implying that the splitting may be much smaller there.

In the following discussion, we would like to emphasize that the experimental results cannot be explained by models that consider a spatially homogeneous layer polarization that goes to zero and reverses in sign when E_F passes through E_D (refs 2,7; blue line in Fig. 4a). As discussed previously, the measured bilayer bandgap remains open, with values on the order of 25 meV even when E_D coincides with E_F. Our measurements demonstrate that both the total charge density and the charge imbalance between the layers fluctuate spatially, reflecting the variation of the disorder potential. This is surprising, as the density range controlled by the external gate ($\Delta V_g = 60$ V corresponds to $\Delta n = \pm 2.2 \times 10^{12}$ cm^{-2}; ref. 28) is significantly larger than the density fluctuations corresponding to potential minima and maxima ($\Delta V_o = 5$ V corresponds to $\Delta n = 3.6 \times 10^{11}$ cm^{-2} see Methods; ref. 28). We suggest that local fields from charged impurities close to the interface between the graphene and the insulator can dominate the local charge imbalances.

We graphically illustrate the charge imbalance and resulting direction of local fields in electron and hole puddles in Fig. 4d. At overall hole doping in the bilayer (leftmost panel), the electron puddles have a large energy asymmetry (red arrow) whereas the asymmetry in the hole puddles becomes small (blue arrow). Here, the sign of the local polarization field coincides with the external field in electron puddles and is opposite in hole puddles. The opposite trend occurs at electron doping in the bilayer, consistent with the reversal of the external electric field at $V_g \gg V_D$ (rightmost panel in Fig. 4d). Importantly, the direction of the local polarization does not follow the direction of the external electric field and must be determined by other factors, such as local fields from impurities or the gradients of the disorder potential, that change sign in different puddles. The schematic also offers a possible simple clue. Over the whole density range, the amplitude of density fluctuations in the bottom layer is larger than that in the top layer, consistent with the screening of the substrate-induced potential disorder. The resulting density schematics, shown as line profiles in Fig. 4d, naturally result in the potential asymmetries and local fields reversing in sign from electron to hole puddles.

Even though we observe a non-zero energy gap when E_D crosses E_F, it is not clear whether the observed asymmetries are related to the broken symmetry states predicted in recent models[11,18,19,34,35], or are the result of the broken symmetry related to the substrate interactions. In contrast, the existence of the subgaps in electron puddles when $LL_{(0,+);(1,+)}$ crosses E_F is possibly related to the recent theoretical predictions of spontaneously broken symmetry states. At present, we are not able to identify the exact quantum numbers of the split $LL_{(0,+);(1,+)}$ levels. However, recent transport measurements point to a pseudospin polarized ground state[13,19,34]. The spontaneously broken symmetry states lead to the opening of a gap due to many-body interactions in zero electric field[13,18,19,34]. In this model, a pseudo-ferromagnetic ground state with fully polarized pseudospins is favoured at small electric fields, which is followed by antiferromagnetic or ferrimagnetic ordering. These effects lead to a non-monotonic dependence of the bandgap on applied electric field, with magnitudes comparable to those observed in this study[18]. However, in realistic devices with disorder, the spontaneous polarization must nucleate with a sign determined by the disorder potential variation.

Methods

The experiments were performed with an ultra-high vacuum (UHV) STM facility at NIST in magnetic fields from 0 to 8 T at a temperature of 4.3 K. The graphene device was fabricated in a similar way to that reported in Novoselov and colleagues[36]. Graphene flakes were mechanically exfoliated from natural graphite and transferred onto thermally grown 300 nm thick SiO_2 on Si. The highly doped Si substrate was used as a back gate to control the charge density of the graphene device. Multiple steps of gold evaporation (50 nm for single deposition) through a SiN stencil mask were implemented to preserve a clean graphene surface. Raman spectroscopy measurements were performed to determine the single and bilayer graphene regions[28]. A two-dimensional piezoelectric actuator was used to position the probe tip on the graphene device with the aid of optical viewing. An iridium probe tip was prepared by *ex situ* electrochemical etching, and cleaned and characterized by *in situ* field ion microscopy before the measurements. STS measurements were performed using a lock-in detection method with a modulation frequency of ≈500 Hz and root-mean-square modulation voltages between 1 and 8 mV, depending on the spectral range of interest. The disorder potential map in Fig. 2c was obtained using closed-loop dI/dV measurements, as described previously[26,28].

dI/dV gate maps were obtained by taking standard open-loop dI/dV spectra, closing the STM servo loop and changing the gate voltage, and then repeating the open-loop dI/dV measurement. The effective mass can be determined from the density dependence of the charge neutrality point in the gate map at zero magnetic field (Fig. 3b). The charge neutrality point can be determined from the centre of the gap (green circles in Fig. 3b), which varies linearly with density as $E_D = \hbar^2 \pi n / 2m^*$ (assuming a density independent mass), in contrast to the square-root dependence in a single layer[28]. Here, the two-dimensional charge-carrier density n is defined

by the applied gate potential, $n = \alpha(V_g - V_o)$, where α is determined by the gate capacitance (300 nm of SiO_2) as 7.19×10^{10} cm^{-2} V^{-1} and V_o is the shift of E_D due to intrinsic doping[28,37,38]. A linear fit (yellow line in Fig. 3b) to E_D with density yields an effective mass $m^* = (0.033 \pm 0.002)m_e$ (all uncertainties reported represent one standard deviation in the measured quantity), where m_e is the electron mass, in agreement with bilayer graphene properties[39]. Using the interlayer coupling constant, $\gamma_1 = 2m^*v_F{}^2 = 0.377$ eV (ref. 39), we can extract the Fermi velocity as $v_F = (1.010 \pm 0.003) \times 10^6$ m s^{-1}. In this puddle the charge neutrality point is close to E_F at a gate voltage of $V_g \approx 30$ V. Spatially, V_o varies from $V_g \approx 30$ V (electron puddles) to $V_g \approx 35$ V (hole puddles).

Received 31 January 2011; accepted 23 March 2011; published online 24 April 2011

References

1. Geim, A. K. & Novoselov, K. S. The rise of graphene. *Nature Mater.* **6,** 183–191 (2007).
2. McCann, E. Asymmetry gap in the electronic band structure of bilayer graphene. *Phys. Rev. B* **74,** 161403 (2006).
3. Guinea, F., Castro Neto, A. H. & Peres, N. M. R. Electronic states and Landau levels in graphene stacks. *Phys. Rev. B* **73,** 245426 (2006).
4. Zhang, Y. *et al.* Direct observation of a widely tunable bandgap in bilayer graphene. *Nature* **459,** 820–823 (2009).
5. Kuzmenko, A. B., Crassee, I., van der Marel, D., Blake, P. & Novoselov, K. S. Determination of the gate-tunable band gap and tight-binding parameters in bilayer graphene using infrared spectroscopy. *Phys. Rev. B* **80,** 165406 (2009).
6. Mak, K. F., Lui, C. H., Shan, J. & Heinz, T. F. Observation of an electric-field-induced band gap in bilayer graphene by infrared spectroscopy. *Phys. Rev. Lett.* **102,** 256405 (2009).
7. Castro, E. V. *et al.* Biased bilayer graphene: Semiconductor with a gap tunable by the electric field effect. *Phys. Rev. Lett.* **99,** 216802 (2007).
8. Xia, F., Farmer, D. B., Lin, Y. & Avouris, P. Graphene field-effect transistors with high on/off current ratio and large transport band gap at room temperature. *Nano Lett.* **10,** 715–718 (2010).
9. Min, H., Sahu, B., Banerjee, S. K. & MacDonald, A. H. *Ab initio* theory of gate induced gaps in graphene bilayers. *Phys. Rev. B* **75,** 155115 (2007).
10. Yan, J. & Fuhrer, M. S. Charge transport in dual gated bilayer graphene with corbino geometry. *Nano Lett.* **10,** 4521–4525 (2010).
11. Shizuya, K. Pseudo-zero-mode Landau levels and collective excitations in bilayer graphene. *Phys. Rev. B* **79,** 165402 (2009).
12. McCann, E. & Fal'ko, V. I. Landau-level degeneracy and quantum Hall effect in a graphite bilayer. *Phys. Rev. Lett.* **96,** 086805 (2006).
13. Weitz, R. T., Allen, M. T., Feldman, B. E., Martin, J. & Yacoby, A. Broken-symmetry states in doubly gated suspended bilayer graphene. *Science* **330,** 812–816 (2010).
14. Feldman, B. E., Martin, J. & Yacoby, A. Broken-symmetry states and divergent resistance in suspended bilayer graphene. *Nature Phys.* **5,** 889–893 (2009).
15. Zhao, Y., Cadden-Zimansky, P., Jiang, Z. & Kim, P. Symmetry breaking in the zero-energy Landau level in bilayer graphene. *Phys. Rev. Lett.* **104,** 066801 (2010).
16. Dean, C. *et al.* Boron nitride substrates for high-quality graphene electronics. *Nature Nanotech.* **5,** 722–726 (2010).
17. Barlas, Y., Côté, R., Nomura, K. & MacDonald, A. H. Intra-Landau-level cyclotron resonance in bilayer graphene. *Phys. Rev. Lett.* **101,** 097601 (2008).
18. Jung, J., Zhang, F. & MacDonald, A. H. Lattice theory of pseudospin ferromagnetism in bilayer graphene: Competing interaction-induced quantum Hall states. *Phys. Rev. B* **83,** 115408 (2011).
19. Nandkishore, R. & Levitov, L. Quantum anomalous Hall state in bilayer graphene. *Phys. Rev. B* **82,** 115124 (2010).
20. Ohta, T., Bostwick, A., Seyller, T., Horn, K. & Rotenberg, E. Controlling the electronic structure of bilayer graphene. *Science* **313,** 951–954 (2006).
21. Zhang, L. M. *et al.* Determination of the electronic structure of bilayer graphene from infrared spectroscopy. *Phys. Rev. B* **78,** 235408 (2008).
22. Oostinga, J. B., Heersche, H. B., Liu, X., Morpurgo, A. F. & Vandersypen, L. M. K. Gate-induced insulating state in bilayer graphene devices. *Nature Mater.* **7,** 151–157 (2008).
23. Zou, K. & Zhu, J. Transport in gapped bilayer graphene: The role of potential fluctuations. *Phys. Rev. B* **82,** 081407 (2010).
24. Taychatanapat, T. & Jarillo-Herrero, P. Electronic transport in dual-gated bilayer graphene at large displacement fields. *Phys. Rev. Lett.* **105,** 166601 (2010).
25. Li, J., Martin, I., Buttiker, M. & Morpurgo, A. F. Topological origin of subgap conductance in insulating bilayer graphene. *Nature Phys.* **7,** 38–42 (2011).
26. Zhang, Y., Brar, V. W., Girit, C., Zettl, A. & Crommie, M. F. Origin of spatial charge inhomogeneity in graphene. *Nature Phys.* **5,** 722–726 (2009).
27. Deshpande, A., Bao, W., Miao, F., Lau, C. N. & LeRoy, B. J. Spatially resolved spectroscopy of monolayer graphene on SiO_2. *Phys. Rev. B* **79,** 205411 (2009).
28. Jung, S. *et al.* Evolution of microscopic localization in graphene in a magnetic field from scattering resonances to quantum dots. *Nature Phys.* **7,** 245–251 (2011).
29. Efros, A. & Shklovskii, B. Coulomb gap and low temperature conductivity of disordered systems. *J. Phys. C* **8,** L49–L51 (1975).
30. Novoselov, K. S. *et al.* Unconventional quantum Hall effect and Berry's phase of 2π in bilayer graphene. *Nature Phys.* **2,** 177–180 (2006).
31. Dial, O. E., Ashoori, R. C., Pfeiffer, L. N. & West, K. W. High-resolution spectroscopy of two-dimensional electron systems. *Nature* **448,** 176–179 (2007).
32. Hashimoto, K. *et al.* Quantum hall transition in real space: From localized to extended states. *Phys. Rev. Lett.* **101,** 256802 (2008).
33. Song, Y. J. *et al.* High-resolution tunnelling spectroscopy of a graphene quartet. *Nature* **467,** 185–189 (2010).
34. Nandkishore, R. & Levitov, L. Dynamical screening and excitonic instability in bilayer graphene. *Phys. Rev. Lett.* **104,** 156803 (2010).
35. Min, H., Borghi, G., Polini, M. & MacDonald, A. H. Pseudospin magnetism in graphene. *Phys. Rev. B* **77,** 041407 (2008).
36. Novoselov, K. S. *et al.* Two-dimensional atomic crystals. *Proc. Natl Acad. Sci. USA* **102,** 10451–10453 (2005).
37. Miller, D. L. *et al.* Observing the quantization of zero mass carriers in graphene. *Science* **324,** 924–927 (2009).
38. Rutter, G. M. *et al.* Scattering and interference in epitaxial graphene. *Science* **317,** 219–222 (2007).
39. Partoens, B. & Peeters, F.M. From graphene to graphite: Electronic structure around the K point. *Phys. Rev. B* **74,** 075404 (2006).

Acknowledgements

We would like to acknowledge M. Stiles, S. Adam, H. Min, A. H. MacDonald and L. Levitov for fruitful discussions and thank I. Calizo and A. Hight-Walker for Raman spectroscopy characterization of the graphene system.

Author contributions

The graphene sample was fabricated by S.J. and N.N.K. STM/STS measurements were performed by G.M.R., S.J., N.N.K. and J.A.S. The data analysis and preparation of the manuscript were performed by G.M.R., S.J., J.A.S., D.B.N. and N.B.Z.

Additional information

The authors declare no competing financial interests. Supplementary information accompanies this paper on www.nature.com/naturephysics. Reprints and permissions information is available online at http://www.nature.com/reprints. Correspondence and requests for materials should be addressed to N.B.Z. or J.A.S.